Marine Research
of the National Academy of Marine Research
ISSN: 2709-6629 (Vol.6 Iss.1)
GPN: 2011200033

DOI: http://dx.doi.org/10.29677/MR.202606_6(1).0006
2026, 6(1), 135-147

Submarine Cable Safety Monitoring and Assessment Technology

Yan-Wei Wu [1*] Hung-Ming Chen [1] Shih-Sheng Hsu [1] Yu-Chi Chang [1] Chih-Wei Yen [1]

[1] *Green Energy and Environment Research Laboratories, Industrial Technology Research Institute, Tainan, Taiwan*

ABSTRACT

Power transmission relies on long-distance submarine cables to deliver electricity to onshore locations. These cables must withstand harsh and complex marine conditions, with statistics showing that 80% of global offshore wind farm insurance claims are related to submarine cables. This article describes the development of a technology to monitor the burial depth of submarine cables in real time to protect them from marine environmental hazards, which are a major cause of damage and insurance claims in marine zones. The method involves creating numerical models of the cable, soil, and seawater, and verifying these models with field data to achieve accurate predictions of burial depth. The study uses historical sea temperature data and machine learning algorithms, notably the random forest model, to predict seabed temperatures, enhancing the accuracy of the models. The technology has been tested and shown to provide precise burial depth measurements, which could be particularly useful for maintaining and monitoring submarine cables in Taiwan's marine zones and assisting in operational decision-making and early warning systems.

Keywords: submarine cable, distributed temperature sensing (DTS), burial depth estimation.

* Corresponding author, e-mail: YWWu@itri.org.tw

Received May 13, 2025, accepted July 23, 2025.

1 INTRODUCTION

With the rapid expansion of offshore wind power installations, the dependence on long-distance submarine cables has also increased. The network pattern of intertwined submarine cables is becoming increasingly common, considering that around 80% of global offshore wind power insurance claims are directly related to submarine cables (El Mountassir & Strang-Moran, 2018). Located in a typhoon- and earthquake-prone region, Taiwan faces even higher requirements for the safety and stability of submarine power transmission. Therefore, developing technologies for rapid and long-distance monitoring of submarine cable conditions has become crucial. In areas where typhoons and earthquakes occur frequently, extreme environmental changes can alter seabed topography, increasing the risks of cable exposure, physical deformation, aging, damage, or even fracture, severely affecting power transmission (Carter et al., 2009). To prevent submarine cables from overheating during wind turbine operation, adjusting the blade pitch to control power generation is a possible mitigation strategy.

In the coastal waters of Western Taiwan, the seabed is frequently scoured due to strong sand wave activity and frequent typhoons (Huang, 2025). This causes significant variations in cable burial depth every year, increasing the risk of exposure and damage, as shown in Figure 1.

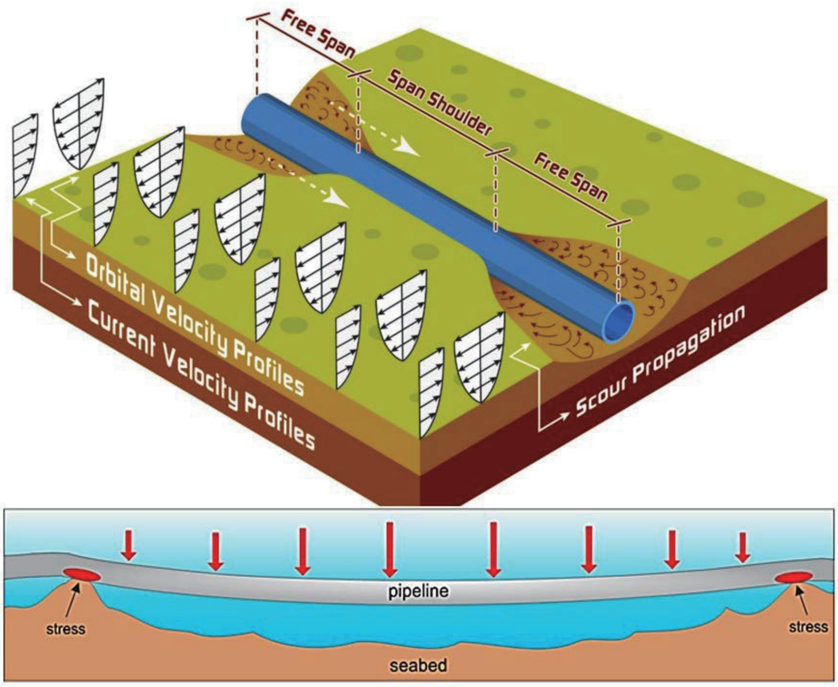

Figure 1. Submarine cable scour caused by external environmental forces.

Traditional surveys require survey vessels and ROVs equipped with sonar sensors to explore cable burial depth along the cable route. This paper proposes using digital sensing technology, embedding optical fibers inside submarine cables as sensors, which enhances the importance of cable burial depth detection. It reduces operation and maintenance costs by lowering the frequency of conventional inspections and intensifying inspections in high-risk areas (Morgan & Slaninka, 1994). Advantages include a stable power supply, reduced cable failure risk, and precise event recording for accountability through continuous digital monitoring.

DOI: 10.29677/MR.202606_6(1).0006

2 RESEARCH METHODS AND OBJECTIVES

This study aims to apply a transient-state submarine cable burial depth computational model to real-world field tests. The inverse model combines critical on-site environmental parameters (seabed temperature, soil thermal conductivity) and monitoring data from the cable (transmission current, fiber-optic monitored temperature), along with the cable's material properties (density, thermal conductivity, and other thermal properties), to conduct inversion analysis and determine actual burial depth. Field experiments verify and improve the accuracy and resolution of the cable burial depth monitoring technique, enhancing cable safety and stability, as shown in Figure 2.

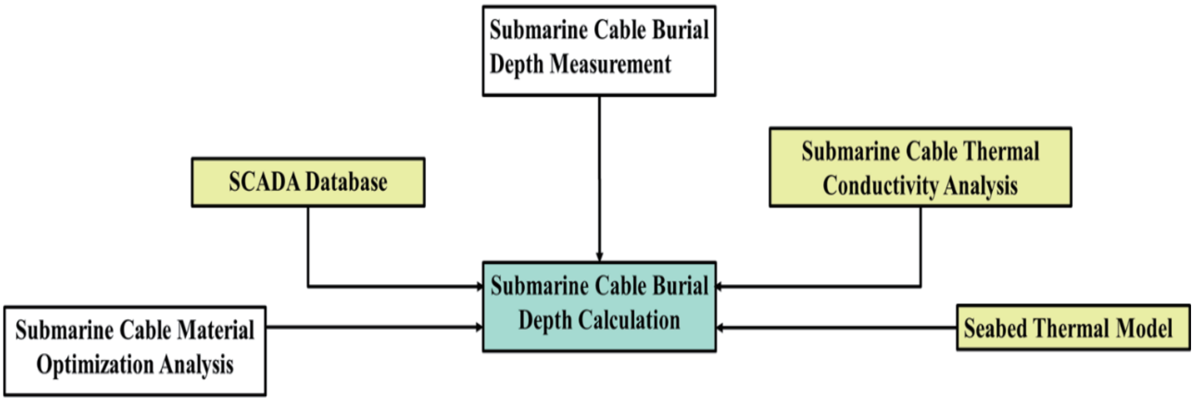

Figure 2. Submarine cable burial depth estimation process.

3 RESEARCH METHODOLOGY

3.1 Data Collection and Analysis

SCADA (Supervisory Control and Data Acquisition) data were obtained from the observation tower of an offshore wind farm, located approximately 6 km off the coast of Changhua at a site with a water depth of 15 meters. Measurements were taken at two depths: 5.4 meters (upper layer) and 13.1 meters (lower layer) below the sea surface. Data were collected every 6 minutes from March 2022 to February 2024 (January and February 2022 data were unavailable). The available data rate exceeds 85% overall, with over 80% availability (Avail) in most months. The average sea temperature ranges from 17°C to 31°C, the upper layer averages 24.94°C, and the lower layer 24.86°C (See Figure 3 and Table 1).

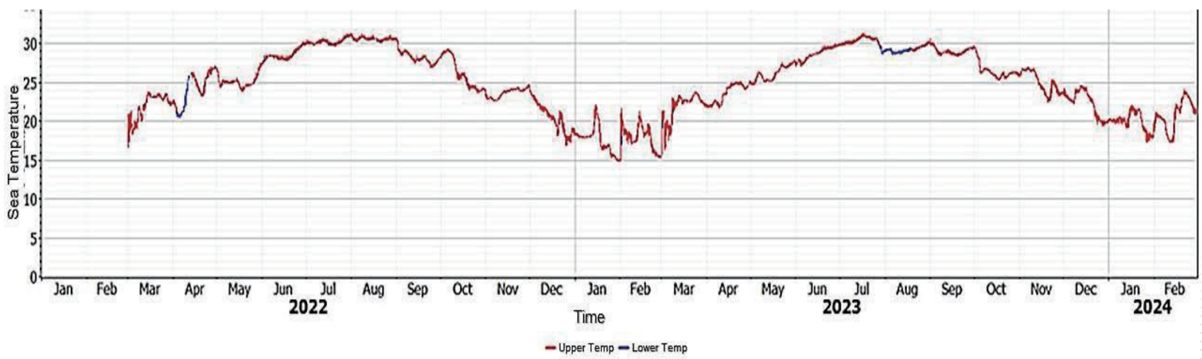

Figure 3. Upper- and lower-layer seawater temperature time series (March 2022 to February 2024).

DOI: 10.29677/MR.202606_6(1).0006

Table 1. Upper- and lower-layer sea temperature statistics (March 2022 to February 2024).

	Upper-Layer Temperature						Lower-Layer Temperature					
Yr	Avail	2022	Avail	2023	Avail	2024	Avail	2022	Avail	2023	Avail	2024
Jan	0.00	-	99.88	17.48	100.0	19.94	0.00	-	99.88	17.47	99.96	19.93
Feb	0.00	-	99.91	17.88	99.91	20.83	0.00	-	99.97	17.84	99.89	20.80
Mar	96.99	21.90	99.80	21.86			96.99	21.92	99.80	21.81		
Apr	66.81	24.99	100.0	23.60			96.43	24.13	99.99	23.59		
May	99.58	25.10	99.97	26.10			81.85	24.84	99.99	26.08		
Jun	99.49	28.50	100.0	28.67			94.35	28.52	100.0	28.64		
Jul	99.73	30.20	88.36	30.36			99.70	30.17	99.99	30.20		
Aug	96.55	30.53	44.21	29.51			93.79	30.50	99.03	29.19		
Sep	100.0	28.14	100.0	28.98			98.25	28.10	100.0	28.95		
Oct	99.48	26.10	99.96	26.38			99.74	26.09	99.99	26.38		
Nov	99.79	23.62	99.88	24.99			99.78	23.62	99.83	24.98		
Dec	100.0	20.52	99.99	22.33			99.96	20.51	99.97	22.32		

Figure 4 shows the correlation analysis of these temperatures, with an R2 value as high as 0.999.

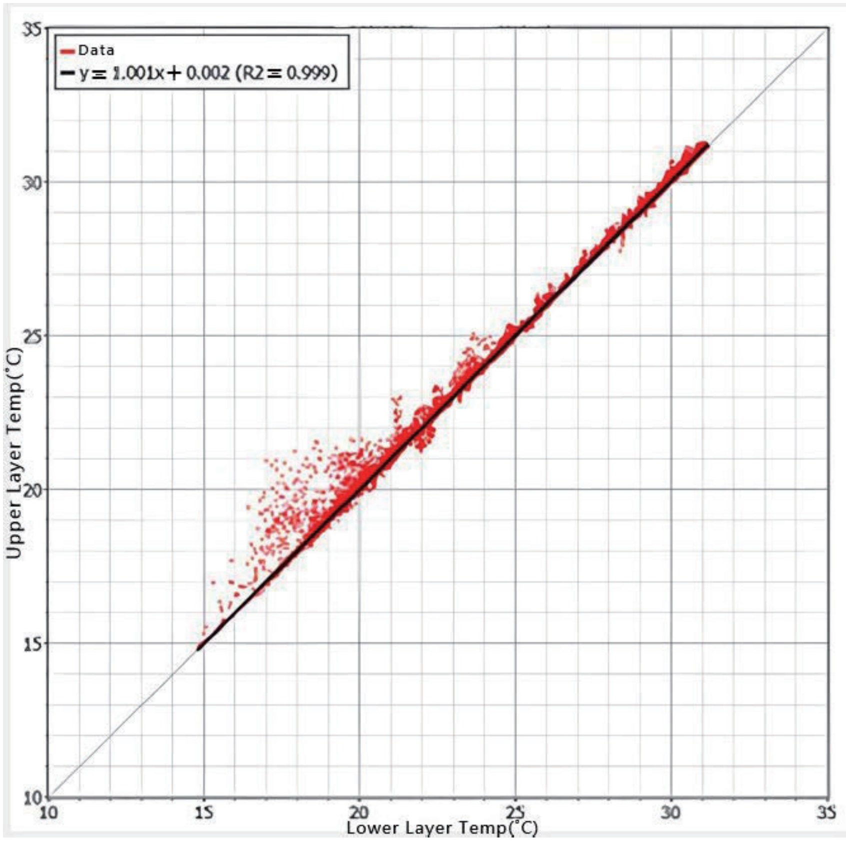

Figure 4. Correlation coefficient analysis of upper- and lower-layer seawater temperature (March 2022 to February 2024).

Marine Research of the National Academy of Marine Research
DOI: 10.29677/MR.202606_6(1).0006

3.2 Seabed Temperature Estimation Model Development

A model was developed to estimate seabed temperature near submarine cables, using upper-layer sea temperature and net solar radiation from the offshore wind farm as inputs, as shown in Table 2.

Due to the ongoing collection of seabed temperature data near the submarine cable, lower-layer seawater temperatures from nearby areas are temporarily used for modeling and algorithm evaluation. The actual data will be integrated once available. The modeling workflow and error analysis are described below:

Table 2. Data for modeling the seabed temperature estimation.

Border	Modeling Data (2022.6–2022.8)	Sampling Frequency
Input	Upper-layer sea temperature, net solar radiation	1 entry every 10 minutes
Output	Lower-layer sea temperature	1 entry every 6 minutes

Let Nr_t, S_t, and D_t represent the net solar radiation, upper-layer seawater temperature, and lower-layer seawater temperature measured at time t (in hours), respectively. All data are converted into multiple sequence pairs (x_i, y_i) as follows:

$$x_i = \left(Nr_{t_i-2.5}, Nr_{t_i-2}, \ldots, Nr_{t_i-0.5}, S_{t_i-2.5}, S_{t_i-2}, \ldots, S_{t_i-0.5}\right) \quad y_i = D_{t_i} \tag{1}$$

The original dataset was transformed into $A = \{(x_i, y_i)\}$. A was randomly split into two subsets: 85% was used as the training set to build models, while the remaining 15% served as the validation set to evaluate the accuracy of each algorithm. Five algorithms, Random Forest, Decision Tree, Support Vector Machine (SVM), XGBoost, and K-nearest neighbors (KNN), were employed for model construction. The goal was to construct a function f such that $f(x_i) \sim yi$. Figure 5 shows each model's error performance on the validation set. The Random Forest model achieved the lowest average error, at only 0.107°C.

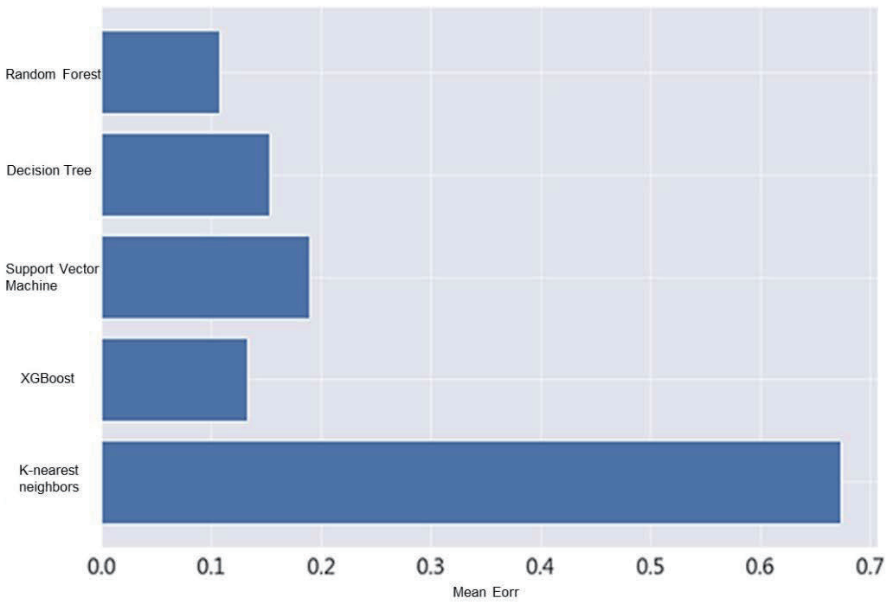

Figure 5. Error analysis for seabed temperature prediction models.

DOI: 10.29677/MR.202606_6(1).0006

3.3 Submarine Cable Model Development

Figure 6 shows that, according to the submarine cable design report, the cable comprises several components, including a copper conductor made of high-conductivity soft copper single wires, twisted and compressed according to the specifications. The conductor must also possess water-blocking functionality (Hughes et al., 2015).

1. Water-Blocked Copper Conductor: Comprised of 19 stranded copper wires with an outer diameter of approximately 8.2 mm. The conductor is made of high-conductivity soft copper single wires, twisted and compressed according to the specifications. The conductor must also possess water-blocking functionality.
2. Conductor Shielding: Made of extruded semi-conductive cross-linked polyethylene material with a minimum thickness of 0.30 mm.
3. XLPE Insulation: Constructed with cross-linked polyethylene (XLPE), concentrically extruded over the conductor shielding layer. The average thickness is 11.0 mm, and the minimum thickness must not exceed 90% of the specified value minus 0.1 mm.
4. Insulation Shielding: Made of extruded semi-conductive cross-linked polyethylene material with a minimum thickness of 0.80 mm.
5. Copper Wires Shielding: Comprising 19 copper wires, each with a diameter of 1.29 mm, wound over a water-blocking non-woven fabric layer.
6. Laminated Metal Tape: A laminated metal tape with a thickness of 0.2 mm; the minimum allowable thickness is 0.17 mm.
7. Inner PE (Polyethylene) Sheath: Black extruded polyethylene material with a thickness of 2.0 mm.
8. Copper Wires Armor: Steel wires with a diameter of 3.4 mm. The armor's designed tensile strength must exceed the tension the cable will experience on the seabed.
9. Outer PE (Polyethylene) Sheath: Black extruded polyethylene material with a thickness of 4.1 mm.

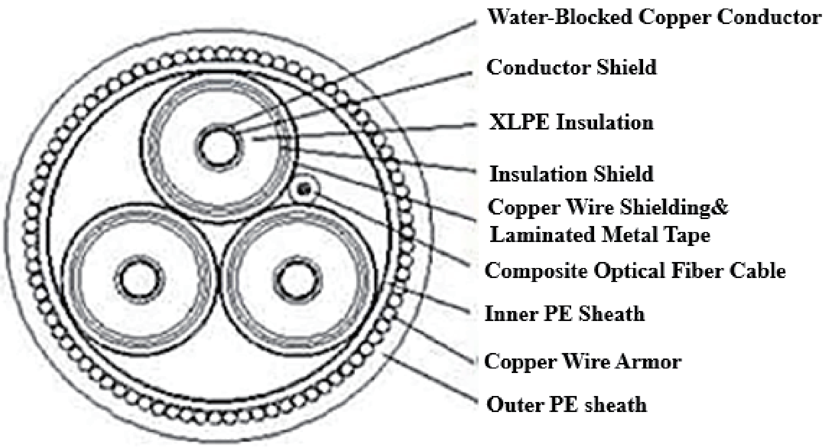

Figure 6. Submarine cable cross-section geometry and material composition according to the design report.

3.4 Optimization of Submarine Cable Material Parameters

A thermo-mechanical coupled model for the submarine cable was constructed to simulate cross-sectional temperature variations caused by changing marine environmental conditions. Based on the submarine cable design report, the geometric properties (such as positions and outer diameters) of each component in the cable cross-section, including the copper conductor, dielectric layer, insulation layer, armor layer, and others, were obtained, along with their material property parameters (thermal conductivity, specific heat capacity, density, etc.), as illustrated in Figure 7.

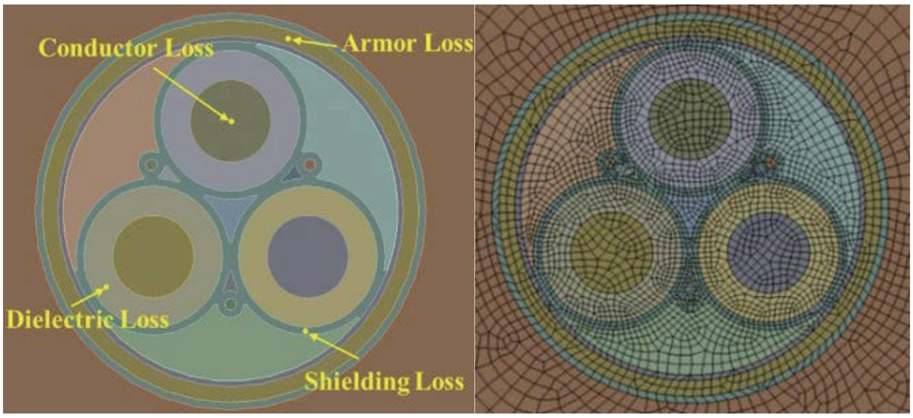

Figure 7. Submarine cable cross-section (left) geometric configuration; (right) mesh generation.

During manufacturing or installation, the submarine cable may undergo deformation due to twisting, insulation material filling, or backfill pressure (Worzyk, 2009). These deformations can cause discrepancies between the assumed parameters in the thermo-mechanical model and real-world conditions. Through optimization analysis, the geometric conditions of the cable cross-section remain unchanged, while material property parameters are fine-tuned to enhance the accuracy and practical applicability of burial depth inversion results. The analysis adheres to the design report's specifications and calibrates the parameters within a reasonable variation range (± 5% error) to account for possible material property deviations.

In addition, the seabed depth and domain boundaries are specified as part of the simulation setup, as shown in Figure 8.

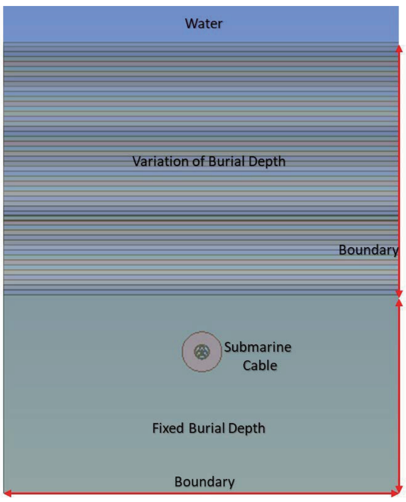

Figure 8. Setup of burial depth and boundaries.

Marine Research of the National Academy of Marine Research
DOI: 10.29677/MR.202606_6(1).0006

3.5 Thermal Loss Analysis of Submarine Cable

The analysis follows the international submarine cable standard IEC 60287-1-1 for thermal loss estimation. According to this standard, the thermal losses in each cable component can be estimated based on their geometric dimensions, the load current, and the conductor temperature. These losses include conductor loss, dielectric loss, shield loss, and armor loss, as outlined below:

$$R' = R_o[1 + \alpha_{20}(\theta - 20)] \tag{2}$$

$$x_s^2 = \frac{8\pi f}{R'} 10^{-7} k_s \tag{3}$$

$$Y_s = \frac{x_s^4}{192 + 0.8x_s^4} \tag{4}$$

$$x_p^2 = \frac{8\pi f}{R'} 10^{-7} k_p \tag{5}$$

$$Y_p = \frac{x_p^4}{192 + 0.8x_p^4} \left(\frac{d_c}{s}\right)^2 \left[0.312\left(\frac{d_c}{s}\right)^2 + \frac{1.18}{\frac{x_p^4}{192 + 0.8x_p^4} + 0.27}\right] \tag{6}$$

R': DC resistance of the copper conductor; d_c: Diameter of the copper conductor; s: Outer diameter of the copper conductor; Y_s: Skin effect factor; Y_p: Proximity effect factor; X_s: Argument of a Bessel function used to calculate skin effect; X_p: Argument of a Bessel function used to calculate proximity effect.

The influence of the skin effect and proximity effect on the transmission line parameters, including resistance, capacitance, and inductance, is incorporated into the loss calculation formula as follows:

$$R = R'[1 + Y_s + Y_p] \tag{7}$$

$$\theta_{SC} = \theta - (I^2R + 0.5W_d)T_1 \tag{8}$$

$$R_s = R_{so}[1 + \alpha_{20}(\theta_{SC} - 20)] \tag{9}$$

$$\lambda_1' = \frac{R_S}{R} \frac{1.5}{1 + (\frac{R_S}{X})^2} \tag{10}$$

$$\lambda_1 = \lambda_1' + \lambda_1'' \tag{11}$$

R: AC resistance of the copper conductor; θ_{SC}: Temperature of the cable shield layer; R_s: AC resistance of the shield layer; λ_1'': Ratio of shield loss to single conductor loss; λ_1: Total ratio of shield loss to conductor loss.

$$\theta_{ar} = \theta - \{(I^2R + 0.5W_d)T_1 + [I^2R(1 + \lambda_1) + W_d]nT_2 \tag{12}$$

$$R_A = R_{Ao}[1 + \alpha_{20}(\theta_{ar} - 20)] \tag{13}$$

$$\lambda_2 = 1.23\frac{R_A}{R}\left(\frac{2c}{d_A}\right)^2 \frac{1}{\left(\frac{2.77R_A 10^6}{\omega}\right)^2 + 1} \tag{14}$$

θ_{ar}: Armor layer temperature; W_d: Dielectric loss; R_A: AC resistance of the armor layer; λ_2: Ratio of armor loss caused by circulating current to conductor loss.

Marine Research of the National Academy of Marine Research
DOI: 10.29677/MR.202606_6(1).0006

4 RESULTS AND DISCUSSION

The accuracy of submarine cable burial depth monitoring technology has been further enhanced by incorporating the temperature monitoring data, environmental observations, seabed temperature estimations, and thermal loss analyses described in Chapter 3.

A calculation process for inferring the burial depth from submarine cable fiber-optic temperature data was established. By comparing the simulated fiber-optic temperature results from the thermo-mechanical coupled model with the actual temperature data returned from fiber-optic monitoring, the burial depth corresponding to the minimum error between the two is identified as the estimated burial depth. The estimated results are then verified against the measured burial depth.

4.1 Field Submarine Cable Burial Depth Survey

Key environmental parameters of the actual submarine cable field sites were collected to establish realistic simulation conditions. The exact burial depth positions of the submarine cable were measured using a sub-bottom profiler, and seabed samples were collected using a grab-type soil sampler. Two survey zones off the coast of Changhua were investigated: 2.5 km offshore, with a water depth of 5 meters in Area A, and 5 km offshore, with a water depth of 12 meters in Area B. The geographic survey data obtained from ship-based measurements conducted by the survey vessel are shown in Figures 9 and 10.

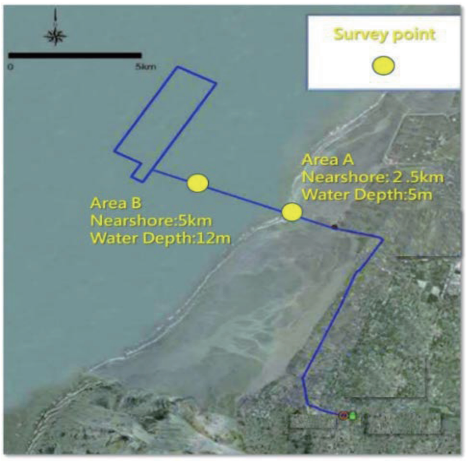

Figure 9. Geographic survey data for submarine cable burial depth investigation.

Figure 10. Survey vessel.

DOI: 10.29677/MR.202606_6(1).0006

The submarine cable burial depth monitoring data in 2024 shows a gradually increasing burial depth trend compared to the previous year. Based on monitoring data from 2023, the average burial depth at 2.5 km offshore was approximately 0.52 meters. At the more distant site, 5 km offshore, the average burial depth exceeds 2 meters, which falls within the safer range according to construction standards and does not require supplementary burial. Only depths below 0.5 meters require reburial, as shown in Figures 11 and 12 and Tables 3 and 4.

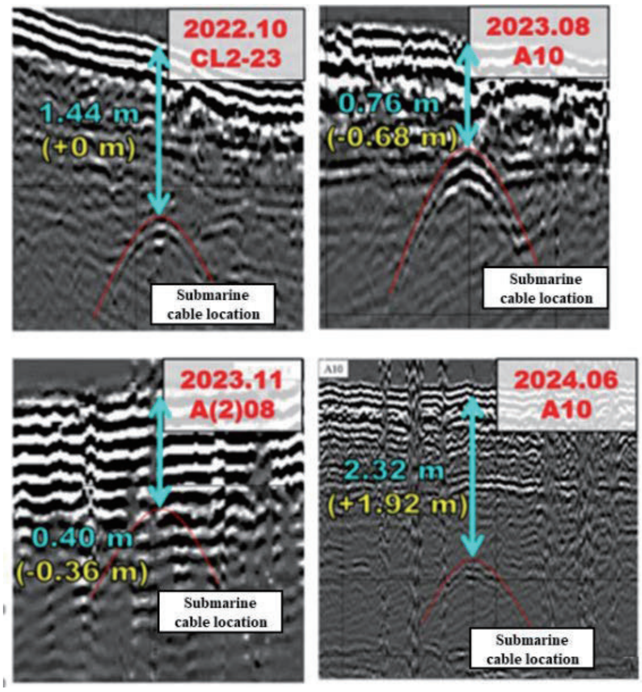

Figure 11. Submarine cable depth profile at Area A (ship-based survey).

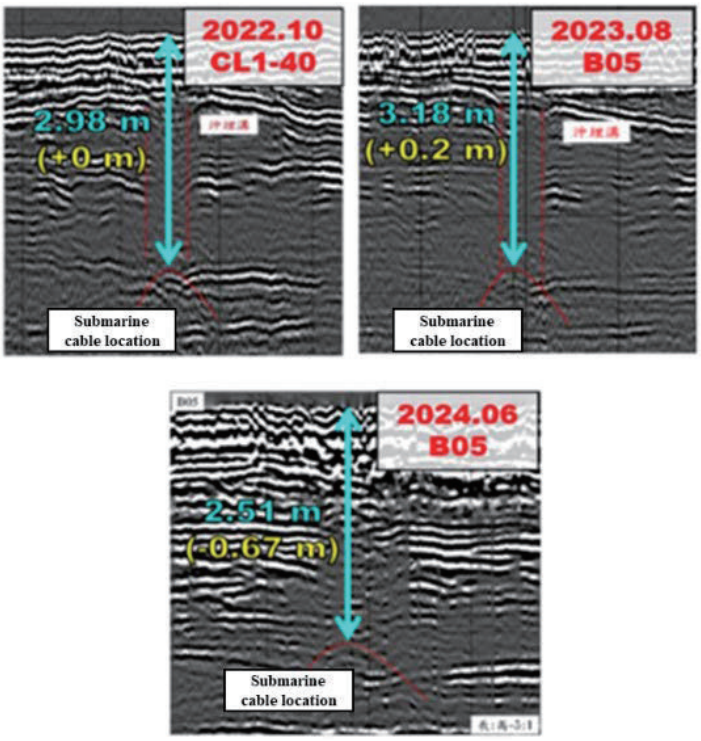

Figure 12. Submarine cable depth profile at Area A (ship-based survey).

DOI: 10.29677/MR.202606_6(1).0006

Table 3. Comparison of burial depths at Area A over the years.

	2022/10	2023/08	2023/11	2024/06
Area A Thickness (m)	1.44 (+0)	0.76 (-0.68)	0.40 (-0.36)	2.32 (+1.92)
Average Thickness (m)	1.97 (+0)	0.99 (-0.98)	0.52 (-0.47)	2.46 (+1.94)

Table 4. Comparison of burial depths at Area B over the years.

	2022/10	2023/08	2023/11	2024/06
Area B Thickness (m)	2.98 (+0)	3.18 (+0.20)	---	2.51 (-0.67)
Average Thickness (m)	2.73 (+0)	3.04 (+0.31)	---	2.42 (-0.89)

4.2 Fiber Optic Temperature Inversion for Burial Depth and Validation

The validation results demonstrate that the burial depth of the submarine cable can be accurately determined by combining SCADA data with a constructed heat transfer model, as well as the 33 kV submarine cable specifications and thermal loss parameters.

In this simulation scenario, the selected conditions correspond to Area A, located 2.5 km offshore, with a still water depth of approximately 5 meters. A burial depth of 0.76 meters, measured during the 2023 ship-based survey, is used as the initial condition. The scenario incorporates the estimated seabed temperature, the measured soil thermal conductivity, the submarine cable load current, and the power plant operator's fiber-optic temperature monitoring data. A steady-state solution method was first applied to back-calculate the soil temperature at the bottom boundary, followed by a transient solution method to compute the burial depth on a 7-day cycle iteratively. The computed burial depths were then compared with and validated against measured data, as illustrated in Figure 13.

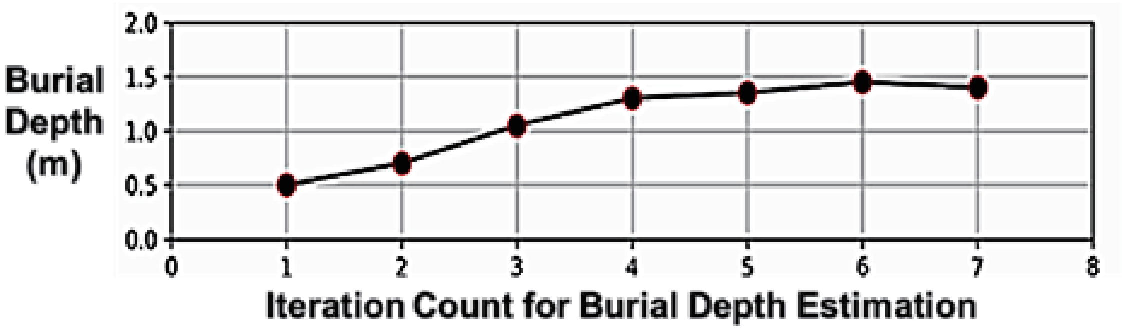

Figure 13. Iteration count for burial depth estimation.

DOI: 10.29677/MR.202606_6(1).0006

Figure 14 shows the 12-week (8/25–11/22) long-term empirical simulation time series. During week 6, strong winds brought by Typhoon Koinu caused the wind turbines to reach full-load operation. As the wind speed further increased beyond the cut-out threshold, the turbines underwent an emergency shutdown, which resulted in a sudden drop in the submarine cable temperature.

The simulated temperatures deviated from the measured values throughout this period, suggesting a burial depth of 0.454 meters. Following the typhoon, the seabed gradually backfilled, and the burial depth exceeded 0.541 meters. As time progressed, the accumulated deviation between simulation and measurement increased. After November, the sampling frequency of the DTS monitoring system was reduced to once per day. In the final week, significant temperature variations were observed under the influence of the northeast monsoon; the final estimated burial depth was 0.49 meters, with an 8-centimeter deviation when compared to the ship-based sub-bottom profiler measurement, which indicated a burial depth of 0.41 (± 0.1 meters).

Figure 14. Simulation results of temperature and burial depth variations at the fiber optic section of the submarine cable in Area A.

5 CONCLUSIONS

This study investigates and validates a digital monitoring technique for estimating the burial depth of submarine cables. An estimation procedure was developed based on analyzing submarine cable load current and fiber-optic temperature data. A machine learning-based inversion method was employed to estimate burial depth, and the results were compared with field measurements to verify the applicability and accuracy of the heat transfer model. A three-month simulation was conducted on an export submarine cable located 2.5 kilometers offshore at a water depth of 5 meters, covering the period from August 22 to November 24, 2023 (12 weeks). The simulated burial depth varied from 0.76 meters to 0.49 meters over a 12-week period. Compared to the final shipborne survey result obtained using a sub-bottom profiler, which indicated a burial depth of 0.41 meters (± 0.1 meters), the deviation was 8 centimeters, demonstrating the high accuracy and practical applicability of the proposed technique.

This technique can accurately predict the burial depth of submarine cables, providing effective burial depth alerts for offshore wind farm operation and maintenance, improving transmission safety, and preventing cable overheating and damage. It also enhances industry competitiveness, improves the operational stability of marine zones, reduces maintenance costs, and promotes the development of the energy sector.

Marine Research of the National Academy of Marine Research
DOI: 10.29677/MR.202606_6(1).0006

ACKNOWLEDGEMENTS

The authors would like to thank the Energy Administration, Ministry of Economic Affairs, Taiwan, for their support under Grant Number 114-D0107.

REFERENCES

Carter, L., Burnett, D., Drew, S., Marle, G., Hagadorn, L., Bartlett-McNeil, D., & Irvine, N. (2009). *Submarine cables and the oceans: Connecting the world.* International Cable Protection Committee; United Nations Environment Programme World Conservation Monitoring Centre. https://doi.org/10.34892/FC3W-X186

El Mountassir, O., & Strang-Moran, C. (2018). *Offshore wind subsea power cables: Installation, operation and market trends.* ORE Catapult. https://ore.catapult.org.uk/resource-hub/analysis-reports/subsea-cable-trends

Huang, K. (2025, March 31). *Strengthening Taiwan's sea cable security.* The Hague Centre for Strategic Studies. https://hcss.nl/report/strengthening-taiwans-sea-cable-security/

Hughes, T. J., Henstock, T. J., Pilgrim, J. A., Dix, J. K., Gernon, T. M., & Thompson, C. E. L. (2015). Effect of sediment properties on the thermal performance of submarine HV cables. *IEEE Transactions on Power Delivery, 30*(6), 2443–2450. https://doi.org/10.1109/TPWRD.2015.2398351

Morgan, V. T., & Slaninka, P. (1994). The external thermal resistance of power cables in a group buried in non-uniform soil. *Electric Power Systems Research, 29*(1), 35–42. https://doi.org/10.1016/0378-7796(94)90046-9

Worzyk, T. (2009). *Submarine power cables: Design, installation, repair, environmental aspects.* Springer. https://doi.org/10.1007/978-3-642-01270-9